Measurements of the ^{48}Ca(γ,n) reaction

J. R. Tompkins, C. W. Arnold, H. J. Karwowski, and G. C. Rich
Department of Physics and Astronomy, University of North Carolina, Chapel Hill, North Carolina 27599, USA and Triangle Universities Nuclear Laboratory, Durham, North Carolina 27708, USA

L. G. Sobotka
Department of Chemistry and Department of Physics, Washington University, St. Louis, Missouri, 63130, USA

C. R. Howell
Department of Physics, Duke University, Durham, North Carolina 27708, USA and Triangle Universities Nuclear Laboratory, Durham, North Carolina, USA 27708

(Received 13 January 2011; revised manuscript received 25 July 2011; published 31 October 2011)

The ^{48}Ca(γ,n) cross section was measured by using γ-ray beams of energies between 9.5 and 15.3 MeV generated at the Triangle Universities Nuclear Laboratory high-intensity γ-ray source. Prior to this experiment, no direct measurements had been made with γ-ray beams of sufficiently low energy spread to observe a structure in this energy range. The cross sections were measured at 34 different γ-ray energies with an enriched ^{48}Ca target. Neutron emission is the dominant decay mechanism in the measured energy range that spans from the threshold, across the previously identified $M1$ strength, and up the low-energy edge of the $E1$ giant dipole resonance. This paper found $B(M1) = 6.8 \pm 0.5\mu_N^2$ for the 10.23-MeV resonance, a value greater than previously measured. Structures in the cross section have been observed whose magnitudes are in agreement with existing data and that are commensurate with extended random-phase approximation calculations.

DOI: 10.1103/PhysRevC.84.044331 PACS number(s): 25.20.−x, 21.60.Jz, 24.30.Cz

I. INTRODUCTION

The investigation of magnetic dipole transitions provides information about the spin and isospin parts of the effective nuclear interaction. It has been observed that the strength distribution of these $M1$ transitions is fragmented in nuclei. Because of recent computational progress, shell-model (SM) studies, performed in large model spaces, are able to describe details of the fragmentation of this mode in pf-shell nuclei. ^{48}Ca is an excellent test case for these studies because of the relatively small fragmentation of the strength distribution and its simple shell structure.

In the independent-particle model, an $M1$ transition in ^{48}Ca is a pure neutron spin-flip excitation from $0f_{7/2} \rightarrow 0f_{5/2}$. In this extreme model, the transition strength is proportional to the number of unmatched spin-orbit nucleons and is equal to $|\langle j = \frac{7}{2}||M1||j = \frac{5}{2}\rangle|^2 = 11.98\mu_N^2$ [1]. For 25 years, it has been known that the strength distribution of the $M1$ transition, which is fragmented throughout the low-energy region, is dominated by a single fragment at 10.23 MeV. This fragment has been observed in (e,e') [2], (p,p') [3–7], and (p,n) as an isobaric analog in ^{48}Sc [8]. The interest in this excitation is not in the location of the major fragment but in its strength [9,10], measured by (e,e') to be $B(M1) = 3.9 \pm 0.3\mu_N^2$ [2]. This strength amounts to approximately $1/3$ of that expected in the independent-particle model. In addition, the summed strength $\Sigma B(M1)$ in the region between 7.7 and 12.7 MeV has been measured to be $5.3 \pm 0.6\mu_N^2$, which accounts for less than $1/2$ of the predicted strength. The general fragmentation, localization at 10.23 MeV, and overprediction of the $\Sigma B(M1)$ by an independent-particle model in the low-energy region of the $M1$ strength distribution all indicate the extent and nature of the complex correlations that exist in nuclei.

Quenching of the $M1$ strength is not surprising as standard intrashell configuration mixing (CM) causes destructive interference between the $0f_{7/2} \rightarrow 0f_{5/2}$ and the $0f_{5/2} \rightarrow 0f_{7/2}$ contributions to the $1p1h$ excitation [11]. This quenching, at the $0\ \hbar\omega$ level, amounts to no more than 25% and, thus, is less than half that required to explain the experimental results cited above. Additional quenching has been found in studies of higher-order CM, which extend beyond the pf shell [12–17]. These papers have indicated that mixing at the $2\hbar\omega$ level is significant, and while contributions at the $4\hbar\omega$ level are small, they are not entirely negligible [12]. Altogether, the inclusion of these effects improves but fails to bring agreement between theory and experiment. Consequently, other sources of quenching and the relocation of $M1$ strength have been proposed [9,12]; these include: CM at the $6\hbar\omega$ level, the effects of short-range correlations, $\Delta(1232)$-nucleon hole coupling, and ρ-meson exchange. All effects beyond the $0\hbar\omega$ level are dealt with phenomenologically in SM calculations by rescaling the free spin operator g_s^{free}.

For the $E1$ strength, random-phase approximation (RPA) calculations in the region of the low-energy edge of the giant dipole resonance (GDR) show multiple sharp peaks in the $E1$ strength distribution [14]. These peaks, which are artificially smoothed for presentation in standard RPA, broaden naturally in extended random-phase approximation (ERPA) calculations caused by the inclusion of coupling to $2p2h$ intra- and intershell configurations: The more the coupling, the smoother the response. Green's function methods, which extend the theory of finite Fermi systems (TFFSs) [18], also

predict this smoothing when coupling of $1p1h$ states to more complex configurations is included [16]. Thus, the presence and magnitude of the structures in the $E1$ strength distribution reflect the importance of such $2p2h$ configurations to the ground-state configuration.

The present paper used real photons to excite $M1$ and $E1$ transitions in an enriched ^{48}Ca sample. The (γ,n) cross section was measured from $E_\gamma = 9.5$ MeV, just below the neutron emission threshold, to 15.3 MeV using a highly efficient Model IV inventory sample counter (INVS) [19] that was adapted for beam experiments. The energy resolution of the beam, which was better than 2.6%, was far superior to that achievable in previous photon work that utilized a bremsstrahlung spectrum [20] and provided the ability to resolve the structures predicted by RPA calculations. At these energies, single-neutron emission is the dominant decay channel, and thus, a deduction of a $B(M1)$ for the strong $M1$ fragment at 10.23 MeV as well as inferences about the $E1$ strength distribution can be made.

II. EXPERIMENTAL SETUP

A. The high-intensity γ-ray source

The high-intensity γ-ray source at Triangle Universities Nuclear Laboratory produced nearly monoenergetic γ-ray beams by means of Compton backscattering inside the optical cavity of a storage-ring-based free-electron laser. Details pertaining to the general operation and capabilities of the facility can be found in Ref. [21]. The beams were circularly polarized and were produced with both high-, $\Delta E_\gamma/E_\gamma = 0.9\%$–$1.6\%$, and low-, $\Delta E_\gamma/E_\gamma = 1.9\%$–$2.3\%$, energy resolutions. The low-resolution beams were used to measure the ^{48}Ca(γ,n) cross section in the energy region $E_\gamma = 9.5$–15.3 MeV in 0.25-MeV steps. Energies at which structure in the cross section was observed were remeasured using high-resolution beams and 0.1-MeV steps.

The γ-ray beams were collimated 60-m downstream from the electron storage ring by a circular aperture of diameter 0.95 cm in a 60-cm-long block of aluminum. Aluminum was chosen to be the material for the primary collimator because it has a high-neutron separation energy $S_n = 13$ MeV. A lead cleanup collimator with a 2.81-cm aperture was positioned downstream of the Al collimator to decrease the flux of small-angle-scattered γ rays from reaching the target, see Fig. 1.

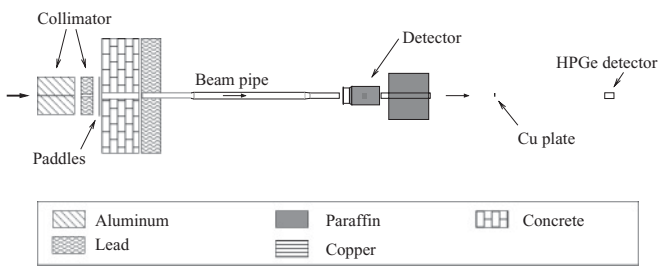

FIG. 1. Scaled diagram of the ^{48}Ca(γ,n) experimental setup. The γ-ray beam direction is indicated by the arrows.

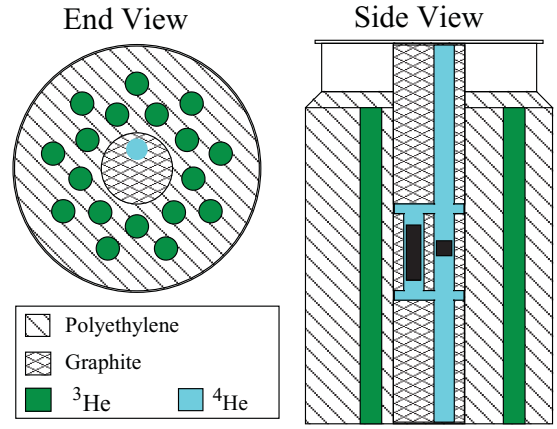

FIG. 2. (Color online) End and side cut-away views of the INVS showing the ^{3}He tubes arranged in two concentric rings around a central cavity filled with three graphite cylinders. The central cylinder holds the four targets (black rectangles) and rotates about the symmetry axis of the detector to change targets.

B. The INVS and targets

Four targets (^{48}Ca, ^{nat}Ca, D_2O, and H_2O) were located in a revolverlike holder in the central cavity of the Model IV INVS counter. The holder was positioned near the center of the INVS to maximize the neutron detection efficiency, which had been measured to be as high as 60% for neutrons with energies below 1 MeV [19]. The detector consists of 18 ^{3}He proportional-counting tubes embedded in a polyethylene moderator, as shown in Fig. 2. All of the tubes are filled with 6 atm of ^{3}He gas. The tubes are arranged into two concentric rings with nine tubes in each. The radius of the inner ring is 7.2 cm, and that of the outer ring is 10.6 cm. Three transistor-transistor logic outputs are produced by the INVS, one for each of the rings and one for the logical OR of the two.

Measurements of ^{48}Ca(γ,n) were obtained with a 92.4%-enriched 2.72-g ^{48}Ca target. A 2.54-cm diameter Plexiglas capsule filled with argon protected the target against oxidation, and low-density foam centered the 1.27-cm diameter × 1.19-cm-long calcium target within the capsule. Contributions to the neutron yield from target impurities and the casing were measured by using a 2.29-g ^{nat}Ca target in an identical casing. The entire data set employs γ rays below the neutron emission threshold of ^{40}Ca, $S_n = 15.6$ MeV.

A 99.9% pure D_2O target, encased in a 7.5-cm-long × 1.92-cm outer diameter polyethylene cylinder with 25.4-μm-thick walls, was used for measurements of the γ-ray flux by means of the ^{2}H(γ,n) reaction. Background contributions from ^{1}H(γ,γ') to this measurement were measured at each γ-ray beam energy by using a second target of identical geometry filled with de-ionized H_2O.

C. Beam diagnostics

The energies of the γ-ray beams were measured at 0.5-MeV intervals by using a high-purity germanium detector positioned in the beam. For these measurements, the beams were

attenuated to less than 4×10^3 γ/s by precision-machined copper blocks prior to collimation. The detector was calibrated with a ^{60}Co source, and confidence in the extrapolated calibration was established by measurement of the sharp $M1$ resonance at 10.23 MeV.

Relative normalization of the flux between different target measurements, which were not concurrent, was made possible by plastic scintillating paddles that remained in the beam at all times.

III. ANALYSIS

A. $B(M1; 0 \rightarrow 10.23$ MeV)

The $B(M1)$ strength can be extracted from the integrated (γ,n) cross section across the resonance by assuming that contributions to the cross section are dominated by the $M1$ resonance. Because the energy width of the γ-ray beam is roughly an order-of-magnitude larger than the upper limit of the resonance width 17 keV [7], transitions nearby are unavoidably excited. A second requirement is that the flux per unit energy across the width of the resonance is constant. This condition is satisfied because the centroid of the beam for one data set was at the resonance energy, and the resonance is sufficiently narrow compared to the energy width of the beam. Finally, the decay mode dominantly must be neutron emission, which is generally true when a nucleus is excited above the particle separation energy. The primary source of uncertainty is in the differential flux of the γ-ray beam at the resonance energy.

The $B(M1)$ can be derived from the rate of neutrons detected from the ^{48}Ca(γ, n) reaction R, where

$$R = n_{48} \int_{\Delta_{\rm res}} \sigma \epsilon \frac{d\phi}{dE_\gamma} dE_\gamma. \quad (1)$$

The quantity ϵ is the efficiency for detecting neutrons, n_{48} is the areal density of ^{48}Ca nuclei exposed to the γ-ray beam, σ is the reaction cross section, and $d\phi/dE_\gamma$ is the differential flux of photons with respect to γ-ray energy. The integration is over the resonance width $\Delta_{\rm res}$. Using both of the assumptions, the equation can be put into the form

$$\frac{R}{n_{48}\epsilon(d\phi/dE_\gamma)|_{E_{\rm res}}} = \int_{\Delta_{\rm res}} \sigma \, dE_\gamma. \quad (2)$$

As discussed in Ref. [1], the $B(M1)$ is related to the right-hand side of Eq. (2) by

$$\int_{\Delta_{\rm res}} \sigma \, dE_\gamma = 4.41 \times 10^{-3} \, E_{\rm res} B(M1) \ {\rm fm}^2 \, {\rm MeV}. \quad (3)$$

Substitution of Eq. (3) into Eq. (2), yields

$$B(M1) = \frac{(2.27 \times 10^2 \ \mu_N^2/{\rm fm}^2) R}{E_{\rm res} n_{48} (d\phi/dE_\gamma)|_{E_{\rm res}} \epsilon}. \quad (4)$$

The differential flux at the resonance energy $d\phi/dE_\gamma|_{E_{\rm res}}$ is determined from the measured γ-ray beam energy profile and total flux by

$$\left.\frac{d\phi}{dE_\gamma}\right|_{E_{\rm res}} = \left.\frac{d\phi^p}{dE_\gamma}\right|_{E_{\rm res}} \frac{\phi^d_{\rm tot}}{\phi^p_{\rm tot}}. \quad (5)$$

TABLE I. The data used in the calculation of the $B(M1; \rightarrow$ 10.23 MeV) along with the result are included in the table.

Quantity	Value	Units
n_{48}	1.92×10^{22}	cm^{-2}
ϵ (0.28 MeV)	$58 \pm 3\%$	absolute
R	610 ± 20	counts/s
$\left.d\phi/dE_\gamma\right\|_{E_\gamma = E_{\rm res}}$	$(3.49 \pm 0.12) \times 10^4$	γ/s/keV
$B(M1; 0 \rightarrow 10.23$ MeV)	6.8 ± 0.5	μ_N^2

The quantity $d\phi^p/dE_\gamma$ is the measured beam energy profile after corrections for an energy-dependent efficiency and detector response have been applied. It is scaled by the ratio of the total flux as measured with the ^{2}H(γ, n) reaction $\phi^d_{\rm tot}$ to the integrated energy profile $\phi^p_{\rm tot}$. The value of each parameter in the $B(M1)$ calculation along with the result are presented in Table I.

B. Cross-sectional determinations

The ^{2}H(γ,n) reaction was used to measure the absolute flux of the incident γ-ray beam. Calculations of the total cross section, which use realistic nucleon-nucleon potentials, such as CD-Bonn, Nijmegen-1, AV18, AV8, and AV6, are considered to be well understood and reliable. For example, the CD-Bonn potential fits world $pp(np)$ data below 350 MeV, up until the year 2000, to a χ^2 per datum of 1.01(1.02) [23]. Further confidence is gained from the fact that all the potentials produce indistinguishable values for the ^{2}H(γ, n) cross section [22] in the energy region of interest, see Fig. 3. For these reasons, a polynomial fit to the CD-Bonn cross sections was used in this analysis.

The ^{48}Ca(γ,n) cross section is determined relative to the ^{2}H(γ,n) cross section as follows:

$$\sigma_{48} = \frac{N_{48}}{N_d} \frac{P_d}{P_{48}} \frac{\epsilon_d}{\epsilon_{48}} \frac{n_d}{n_{48}} \sigma_d, \quad (6)$$

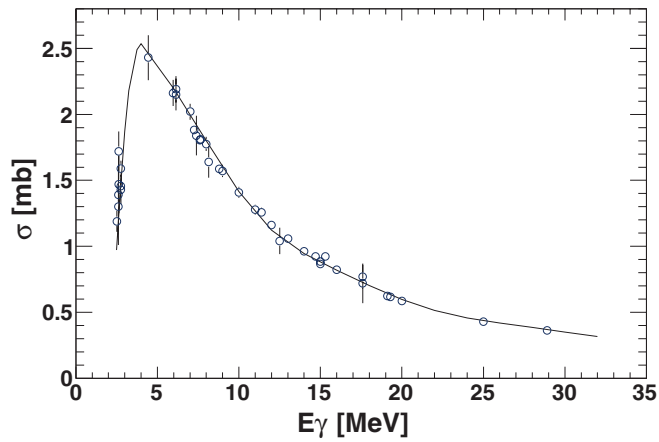

FIG. 3. (Color online) Theoretical calculations of the ^{2}H(γ, n) total cross section (solid curve) and data (open circles) (figure taken from Ref. [22]). The solid curve represents the overlay of the results of five realistic calculations, which are shown as indistinguishable.

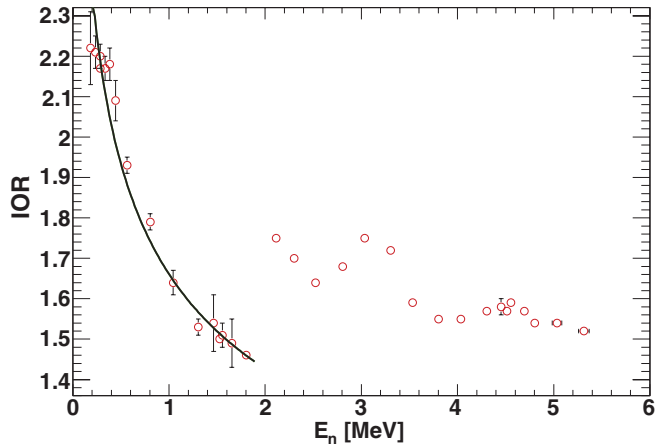

FIG. 4. (Color online) An energy-dependent fit (solid curve) to the ^{48}Ca IOR (open circles) from S_n to 12 MeV, the energy at which decay to the first excited state in ^{47}Ca becomes energetically allowed, was used to determine average neutron energies.

where σ is the total photodisintegration cross section, N and P are the total counts in the INVS and the paddle, respectively, corrected for background counts, ϵ is the neutron detection efficiency, and n is the areal density of the target exposed to the beam. The subscripts d and 48 correspond to the ^{2}H and ^{48}Ca target nuclei, respectively. No correction to these data for the energy shape of the γ-ray beam has been applied, and thus, each point is to be considered an average cross section over the width of the beam.

The INVS was characterized with both simulation and experiment [19]. The neutron detection efficiencies were measured experimentally for energies below 2 MeV and were used to validate the simulations performed with the MCNPX code [24]. The agreement between these enabled the confident extrapolation of the simulated efficiencies for low-energy neutrons to those with higher energy, such as the neutrons produced by the ^{2}H(γ,n) reaction. The characterization procedures were tailored to account for differences in the neutron angular distributions and energetics between the ^{48}Ca(γ,n) and the ^{2}H(γ,n) reactions.

The emitted neutrons from the photodisintegration of ^{48}Ca at $E_\gamma > 12.0$ MeV are not monoenergetic. However, the energy distribution is well represented by the average $\langle E_n \rangle$, and a detection efficiency that corresponds to $\langle E_n \rangle$ was used. This efficiency was determined from the MCNPX simulation and was defined as $\epsilon = n_{\rm dis}/n_{\rm ini}$ where $n_{\rm dis}$ is the number of neutron disappearances in the active volume of the ^{3}He tubes and $n_{\rm ini}$ is the number of initial neutrons. The ratio of neutron counts in the inner ring to those in the outer, now referred to as the inner-to-outer ratio (IOR), was used to determine $\langle E_n \rangle$. For $E_\gamma < 12.0$ MeV, the energy dependence of the ratio could be fit with a single power law, see Fig. 4, whose inversion was used to determine $\langle E_n \rangle$ for all relevant E_γ.

The $\langle E_n \rangle$ determined with the IOR technique described above was validated by using the statistical model code GEMINI++ [25]. In this code, the decay of an excited nucleus with $J^\pi = 1^-$ to all energetically allowed known states with $J \leqslant 9/2$ in ^{47}Ca [26] was calculated by using the Hauser-Feshbach formalism. Decays of excited 1^+ states were not considered because of their very small $M1$ transition strengths [2]. The fractional contribution of each decay channel was computed and was used with the corresponding detection efficiencies to form the weighted average of the neutron detection efficiency at a given E_γ. The result was compared with that of the IOR technique, and reasonable agreement was found, see Fig. 5. Further validation, which used the full reaction model code, TALYS [27], produced similar results. A relative uncertainty of $\pm 5\%$ is assigned to the efficiency determination because of the assumption about the angular distribution and the fact that the neutron detector efficiency is angular dependent when $E_n > 0.5$ MeV [19].

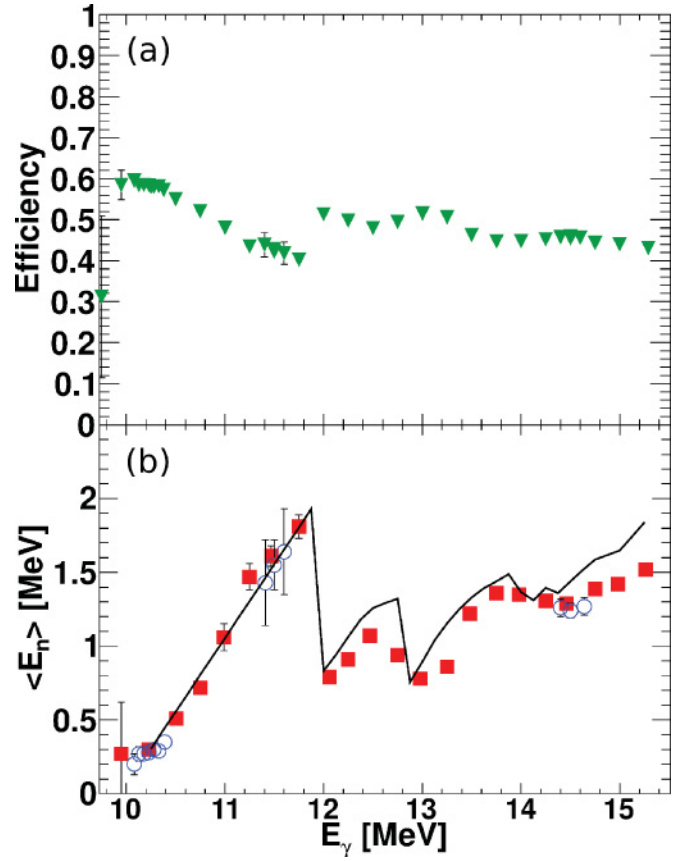

FIG. 5. (Color online) (a) The efficiency for detecting neutrons from the ^{48}Ca(γ, n) reaction at a given E_γ is plotted (triangles). (b) The $\langle E_n \rangle$ at each γ-ray beam energy as determined by GEMINI++ (solid curve) and by using the IOR technique for the high- (circles) and low- (squares) resolution data. Uncertainties presented reflect statistical uncertainties only.

The procedure for characterizing the detector's response to neutrons from deuteron photodisintegration accounted for the known $\sin^2\theta$ angular distribution [28]. The associated kinematics were accounted for with the following equation:

$$\epsilon(E_\gamma) = \int_0^\pi \epsilon[\theta, E_n(E_\gamma, \theta)] W(\theta) d\theta, \qquad (7)$$

where $W(\theta) = \sin^2\theta$, θ is the polar angle measured with respect to the γ-ray beam, and $E_n(E_\gamma, \theta)$ is the energy of the emitted neutron. The angle- and energy-dependent efficiencies

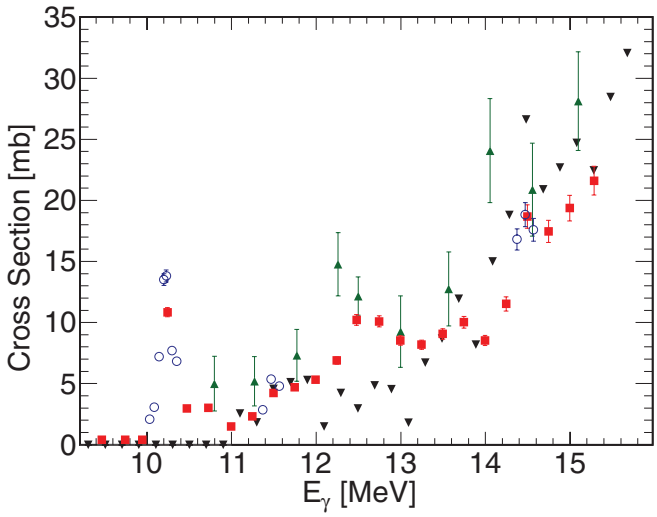

FIG. 6. (Color online) ^{48}Ca(γ, n) total cross section measured with low- (squares) and high- (circles) resolution γ-ray beams. The uncertainties reflect the contributions of systematic uncertainties in the neutron detection efficiency. The upward pointing triangles are the data of Ref. [20] and the inverted triangles are the converted data of Ref. [29].

were the result of simulated monoenergetic conical sources of neutrons for angles $0 < \theta < \pi$ for all neutron energies. A relative uncertainty of $\pm 3\%$ is assigned to the neutron detection efficiency as it pertains to this reaction in concordance with Ref. [19].

The ^{48}Ca(γ,n) cross section, determined by using Eq. (6) as described above, is shown in Fig. 6. The errors on the data points include statistical uncertainties as well as systematic uncertainties in the efficiency for detecting neutrons from the ^{48}Ca(γ,n) reaction.

IV. RESULTS AND DISCUSSION

This paper presents a different technique to extract localized $M1$ strength. As $M1$ and $E1$ are indistinguishable by the detection method, prior knowledge of the distribution of strength in the region and its magnitude is required. Any sizable contribution to neutron counts caused by strength near the major $M1$ resonance or within 9 keV of the peak, which if present would have remained unresolved by any measurement to date, weakens the validity of the $B(M1)$ value extracted by this technique. However, the case of ^{48}Ca is ideal because high-resolution (p, p') experiments show excitable transitions within the experimental energy spread at $E_\gamma = 10.23$ MeV to be small. The relative contributions of these transitions on either side of the resonance, see Fig. 12 of Ref. [30], have been estimated by using a simple model of the spectrum, which uses 3 gaussians, and their combined contribution was found to be on the order of 1% to 2%, see Table II. Thus, the validity of the extraction method is retained.

The applicability of this technique is also dependent on $\Gamma_\gamma \ll \Gamma_n$ because this assumption is implied in Eq. (3). In ^{48}Ca, the radiative decay width of the excited state has a Moszkowski estimate [31] of 35 eV when deexcitation from the $0f_{5/2}$ to the $0f_{7/2}$ level is considered. It is clear that, even if the true width of the peak was an order of magnitude narrower than the 17-keV upper limit, the radiative partial width would be smaller than the total width by a factor of 50.

TABLE II. Estimation of peak contributions to the total neutron counts at the base of the large $M1$ resonance. This estimation includes weighting of the peak heights taken from Fig. 12 of Ref. [30] by the intensity profile of the γ-ray beam. These estimates are upper limits because it has been assumed that any excitation of these levels results unambiguously in a neutron emission.

E_γ (MeV)	Fractional contribution
10.15	0.006
10.23	0.98
10.30	0.011

The above-mentioned estimate concerns undetected strength, which results from the insensitivity of the detector to γ rays. Any strength associated with radiative decay would only increase the difference between the (e, e') result and the present. A $B(M1)$ for the absorption can be calculated from the Moszkowski estimate to be $2.1\mu_N^2$ by using the relationship,

$$B(M1) = \frac{9}{16\pi}\frac{2I_x+1}{2I_0+1}\frac{(2m_pc^2)^2}{\alpha}\frac{1}{E_\gamma^3}\Gamma_\gamma(M1) \qquad (8)$$

derived from Ref. [1]. $B(M1)$ is the transition strength for photoabsorption $I_0 = 7/2$ and $I_x = 5/2$. Although this is a substantial value, it should be considered an upper limit since the Moszkowski estimate itself is crude and likely is an overestimation of the partial width because it neglects the fact that the $0f_{7/2}$ level to which the nucleus decays is nearly full. Empirically, $M1$ photon decay is more than an order of magnitude slower than the Moszkowski estimate. Even with only an order of magnitude retardation, the photon contribution would be substantially less than our uncertainty.

The result from this paper is that the $B(M1)$, in the region of 10.23 MeV, is $6.8 \pm 0.5\mu_N^2$, a value roughly 70% more than the previous result of Steffen *et al.* [2]. The quoted uncertainty is dominated by the uncertainty in the flux and the neutron detection efficiency. This difference is outside of the statistical uncertainties. The results from the (π, π') reaction provide some weak support for the greater suppression, see Ref. [9].

By turning to theory, the ERPA calculations of Brand *et al.* [13–15], which include the $2p2h$ correlations, predict the localized $B(M1)$ at 10.23 MeV to be $6.6\mu_N^2$ with very little additional strength in the 7.7–12.7 MeV energy range. While these calculations agree with the present results, it is expected that the inclusion of short-range correlations and a stronger coupling of $1p1h$ to $2p2h$ states would cause additional fragmentation. This could lead to enough quenching of the low-lying strength to come into agreement with the (e,e') results [32].

As mentioned in Sec. I, CM at the $0\hbar\omega$ level reduces the expected $B(M1)$ by 25%. Thus, for example, the total $B(M1) = 8.96\mu_N^2$ is calculated by using the code ANTOINE [33], which used the effective KB3 interaction [34] and free g-factors g^{free}. This value is still 70% greater than the

experimentally measured value, and the difference is often accounted for by the rescaling of the free spin g-factor. ANTOINE predicts the total $B(M1) = 5.1\mu_N^2$ when using the KB3 interaction but with an effective g-factor $g_s^{\text{eff}} = 0.75 g_s^{\text{free}}$ [33]. The result is in rough agreement with the (e, e') data.

Another SM calculation [35], which uses the GXPF1 interaction does not predict ground-state transition strengths but rather magnetic dipole moments. It reliably reproduces the experimental data for the pf-shell nuclei, up to Ni and Zn with some exceptions, which do not include ^{48}Ca, by using the free spin and free orbital g-factors. The ability of this pf-shell calculation to reproduce the experimentally measured magnetic dipole moments without scaling the free g-factors is similar to the calculations of the sd shell.

An altogether different approach, based on the TFFSs, extends the RPA by coupling $1p1h$ states to the most collectivized phonons ($2p2h$) and the continuum [16]. These calculations are also dependent on effective spin g-factors. The authors found that, for the ^{48}Ca $M1$ resonance, $B(M1) = 8.64\mu_N^2$, $6.55\mu_N^2$, and $6.12\mu_N^2$ when considering coupling of $1p1h$ to the continuum, to $2p2h$ and the continuum with RPA-like ground-state correlations, and to the same with additional ground-state correlations, respectively [17,36]. The present result is in agreement with the calculations that include RPA-like correlations as well as coupling to the continuum and $2p2h$.

The value of the g_s^{eff} hinges on whether there is a persistence of the systematic difference between the $M1$(spin) and the Gamow-Teller (GT) operators, a difference known to exist in the sd-shell nuclei and associated with meson exchange currents [10]. It follows that, if $g_s^{\text{eff}} \approx g_s^{\text{free}}$, the difference is assumed to persist in the pf shell, and if $g_s^{\text{eff}} \approx 0.75 g_s^{\text{free}}$, it vanishes. The work of Towner provides some support for the latter conclusion [37].

Finally, the Monte Carlo SM calculations [38] quench the spin operator (for both the GT and the spin parts of the $M1$) by 0.77, intermediate to the cases above, but far closer to the lower value as it appears as a square in the $B(M1)$. The variance in the theoretical results is an indication of the uncertainty of the magnitude of beyond 0 $\hbar\omega$ effects and provides further incentive to understand the difference between the present results and those from (e, e').

By turning to the remainder of the (γ, n) excitation function, these data provide the highest-resolution study by using real photons above the particle emission threshold in existence and are in near agreement with the data of Ref. [20], see Fig. 6. A comparison of $dB(E1)/dE$ data [29], converted to a total photoabsorption cross section, in accordance with Eq. (9) of Ref. [39], has also been included under the assumption of purely $E1$ transitions. The conversion was computed for each energy bin of the $dB(E1)/dE$ data by using a $B(E1)$ value associated with the energy of the bin center, obtained by integration of $dB(E1)/dE$ over the 200-keV bin width. By excluding the region between $E_\gamma = 12$ and 13 MeV, the results are in accord with the present data. The experimental structure can be compared to that predicted by microscopic calculations. Both the calculations of Brand *et al.* (see Fig. 15d of Ref. [14]) and Kamerdzhiev *et al.* (see Fig. 3.2 of Ref. [36]) show structure commensurate to what is observed. The experimentally observed plateaus at 12.5 and 14.5 MeV have corresponding structures in the ERPA calculations. More fracturing of the strength, which leads to a substantially smoother response, does not seem to be indicated.

V. CONCLUSIONS

Nearly monoenergetic γ-ray beams have been utilized to study the $M1$ and $E1$ strengths in ^{48}Ca between 9.5 and 15.3 MeV. The examined energy region includes the dominant $M1$ fragment at 10.23 MeV and the leading edge of the GDR. The $B(M1)$ was measured to be $6.8 \pm 0.5\mu_N^2$, a value substantially greater than that measured with (e, e'). The result has multiple implications; the first is that the quenching in ^{48}Ca is similar to that found in ERPA calculations, which do not include the effects of short-range correlations. The second is that the difference could be caused by an effective spin operator that is intermediate to those used in the GXPF1 interaction and KB3 interactions. Finally, it implies that meson exchange effects, which generate a difference in the GT and spin $M1$, are still somewhat active in ^{48}Ca. Since, at present, this difference is not understood, further experimental work is required.

ACKNOWLEDGMENTS

We would like to thank the National Superconducting Cyclotron Laboratory for loaning the ^{48}Ca target. We would also like to acknowledge discussions and communications with Dr. B. A. Brown, Dr. I. Towner, Dr. W. H. Dickhoff, Dr. A. Tamii, and Dr. S. Strauch. This work was supported by the US Department of Energy, Division of Nuclear Physics, under Grants No. DE-FG52-06NA26155, No. DE-FG02-97ER41033, No. DE-FG02- 87ER-40316, and NSF/DHS Grant No. 2008-DN-077-ARI014.

[1] A. Bohr and B. Mottelson, *Nuclear Structure* (W. A. Benjamin Inc., New York, 1969), Vol. I, pp. 337, 382; A. Bohr and B. Mottelson, *Nuclear Structure* (W. A. Benjamin Inc., Reading, MA, 1975), Vol. II, p. 477.

[2] W. Steffen, H. D. Gräf, A. Richter, A. Härting, W. Weise, U. Deutschmann, G. Lahm, and R. Neuhausen, Nucl. Phys. A **404**, 413 (1983).

[3] G. P. A. Berg *et al.*, Phys. Rev. C **25**, 2100 (1982).

[4] K. E. Rehm, P. Kienle, D. W. Miller, R. E. Segel, and J. R. Comfort, Phys. Lett. B **114**, 15 (1982).

[5] Y. Fujita, M. Fujiwara, S. Morinobu, T. Yamazaki, T. Itahashi, S. Imanishi, H. Ikegami, and S. I. Hayakawa, Phys. Rev. C **25**, 678 (1982).

[6] G. M. Crawley, N. Anantraman, A. Galonsky, C. Djalali, N. Marty, M. Morlet, A. Willis, and J. C. Jourdain, Phys. Lett. B **127**, 322 (1983).

[7] A. Tamii *et al*., Nucl. Phys. A **788**, 53 (2007).
[8] B. D. Anderson, J. N. Knudson, P. C. Tandy, J. W. Watson, R. Madey, and C. C. Foster, Phys. Rev. Lett. **45**, 699 (1980).
[9] A. Richter, Prog. Part. Nucl. Phys. **13**, 1 (1985).
[10] A. Richter, Prog. Part. Nucl. Phys. **44**, 3 (2000).
[11] A. Arima and H. Horie, Prog. Theor. Phys. **11**, 509 (1954).
[12] K. Takayanagi, K. Shimizu, and A. Arima, Nucl. Phys. A **481**, 313 (1988).
[13] M. G. E. Brand, K. Allaart, and W. H. Dickhoff, Phys. Lett. B **214**, 483 (1988).
[14] M. G. E. Brand, K. Allaart, and W. H. Dickhoff, Nucl. Phys. A **509**, 1 (1990).
[15] M. G. E. Brand, Ph.D. thesis, University of Amsterdam, 1990 (unpublished).
[16] S. P. Kamerdzhiev and V. N. Tkachev, Z. Phys. A **334**, 19 (1989).
[17] S. Kamerdzhiev, J. Speth, G. Tertychny, and J. Wambach, Z. Phys. A **346**, 253 (1993).
[18] A. B. Migdal, *Theory of Finite Fermi-Systems* (Wiley, New York, 1967).
[19] C. W. Arnold, T. B. Clegg, H. J. Karwowski, G. C. Rich, J. R. Tompkins, and C. R. Howell, Nucl. Instrum. Methods Phys. Res. A **647**, 55 (2011).
[20] G. J. O'Keefe, M. N. Thompson, Y. I. Assafiri, and R. E. Pywell, Nucl. Phys. A **469**, 239 (1987).
[21] H. R. Weller, M. W. Ahmed, H. Gao, W. Tornow, Y. K. Wu, M. Gai, and R. Miskimen, Prog. Part. Nucl. Phys. **62**, 257 (2009).
[22] R. Schiavilla, Phys. Rev. C **72**, 034001 (2005).
[23] R. Machleidt, Phys. Rev. C **63**, 024001 (2001).
[24] J. S. Hendricks *et al*., LANL Report No. LA-UR-05-2675, 2005 (unpublished).
[25] R. J. Charity *et al*., Nucl. Phys. A **483**, 371 (1988).
[26] T. W. Burrows, Nucl. Data Sheets **107**, 1747 (2006).
[27] A. J. Koning, S. Hilaire, and M. C. Duijvestijn, in *TALYS: Comprehensive Nuclear Reaction Modeling*, edited by R. C. Haight, M. B. Chadwick, T. Kawano and P. Talou, AIP Conf. Proc. **769** (AIP, New York, 2005), p. 1154.
[28] K. E. Stephenson, R. J. Holt, R. D. McKeown, and J. R. Specht, Phys. Rev. C **35**, 2023 (1987).
[29] S. Strauch, Nucl. Phys. A **649**, 85c (1999).
[30] A. Tamii *et al*., Nucl. Instrum. Methods Phys. Res. A **605**, 326 (2009).
[31] S. A. Moszkowski, *Alpha-, Beta-, and Gamma-Ray Spectroscopy* (North-Holland, Amsterdam, 1965), pp. 863–886.
[32] W. H. Dickhoff (private communication).
[33] P. von Neumann-Cosel, A. Poves, J. Retamosa, and A. Richter, Phys. Lett. B **443**, 1 (1998).
[34] G. Martinez-Pinedo, A. P. Zuker, A. Poves, and E. Caurier, Phys. Rev. C **55**, 187 (1997).
[35] M. Honma, T. Otsuka, B. A. Brown, and T. Mizusaki, Phys. Rev. C **69**, 034335 (2004).
[36] S. Kamerdzhiev, J. Speth, and G. Tertychny, Phys. Rep. **393**, 1 (2004).
[37] I. S. Towner, Phys. Rep. **155**, 263 (1987).
[38] S. E. Koonin, D. J. Dean, and K. Langanke, Phys. Rep. **278**, 1 (1997).
[39] E. F. Gordon and R. Pitthan, Nucl. Instrum. Methods **145**, 569 (1977).